Brownian dynamics of emulsion film formation and droplet coalescence

Jhoan Toro-Mendoza* and Dimiter N. Petsev†
Department of Chemical and Nuclear Engineering, University of New Mexico, Albuquerque, New Mexico 87131, USA
(Received 30 December 2009; revised manuscript received 24 February 2010; published 18 May 2010)

We analyze the evolution in thickness and radius of the film formed during the collision of two deformable emulsion Brownian droplets. These variables exhibit random fluctuations due to thermal disturbances from the continuous liquid phase. As a result, the system probes a random trajectory in the configurational space until it reaches a critical film thickness, at which point the droplets coalesce. Therefore, the film is modeled as a disk with thicknesses and radi that can fluctuate. Our analysis is based on a Langevin-Brownian dynamics approach, which accounts for the thermodynamic and hydrodynamic interactions in the lubrication approximation. We examine the effect of parameters such as droplet size, interfacial mobility, and electrolyte concentration on the coalescence of small Brownian droplets. The results suggest that the coalescence times depend on a complex interplay between the thermodynamic and hydrodynamic interactions.

DOI: 10.1103/PhysRevE.81.051404 PACS number(s): 82.70.Kj, 47.55.df, 47.55.dk, 83.10.Mj

I. INTRODUCTION

Emulsions are colloidal dispersions consisting of droplets suspended in another liquid. The droplet size may vary from tens of nanometers to millimeters or more. These systems are thermodynamically unstable due to the unfavorable free energy contribution associated with the large interfacial area between the droplets and the continuous phase. That is why emulsions tend to phase separate. The addition of surfactant may slow down the phase separation by lowering the interfacial free energy through adsorption and providing additional electrostatic or steric stabilization at the interface [1]. Emulsions are usually kinetically stable, and the average lifetime is an important characteristic that determines their potential use for different applications. The specific phase-separation pathways involve collision between the droplets, subsequent flocculation, and coalescence. Droplet coalescence is the first step that leads to macroscopic phase separation. It is a rather complex event and is an object of a significant fundamental interest in addition to its great practical importance.

The phase-separation kinetics for large droplets (larger than a few micrometers) is dominated by gravity since the two liquids usually have different densities [2]. In contrast, the dynamics of smaller droplets is dominated by Brownian motion. Therefore, the coalescence kinetics is that of a diffusion-controlled reaction. The kinetics of such reactions was first analyzed by Smoluchowski, who investigated the coagulation rate of solid colloidal particles in suspension [3–5]. His analysis was later subject to a number of refinements and improvements [6–14], some of which included density and correlation effects [15–17] or lack of thermal equilibrium [18].

The dynamics of droplet coalescence is more complicated than that of solid particle coagulation [19–21] due to the fact that the droplet interfaces are deformable and may also have tangential mobility. Because of these two features, two colliding deformable droplets may first flocculate, forming a thin liquid film that then thins and finally breaks, leading to merging [22,23]. Sometimes, a liquid bridge may form between the two droplets [24,25]. All these stages contribute to the overall coalescence time. There is experimental evidence which shows that droplet deformability and film formation indeed affect the kinetic stability of emulsions [26–29]. The physical reason for this is that both the direct and hydrodynamic interactions are sensitive to the shape of the approaching droplets [30–38]. In addition, the interfacial mobility of the droplets also has an effect on the hydrodynamic resistance upon approach [39].

The random nature of the coalescence of large droplets has been demonstrated by experiments [40–42] and studied theoretically [29,43,44]. The surface waves produced by the momentum exchange with the surrounding molecules, the hydrodynamic instabilities, and the gradient in surface concentration of surfactant (Marangoni effect) are the major mechanisms responsible for the film rupture [45,46]. New experimental developments allow for the observation of the surface shape fluctuations in large films [47,48]. These variations become more important at high volume fractions because the close packing increases the contact surface due to the deformability of the particles [49–51]. Most of the studies referred above are for large drops with diameters within the range of tens of micrometers to millimeters.

In order to account for the deformability and interfacial mobility effects on the coalescence kinetics of small Brownian droplets, one needs to generalize the Smoluchowski approach [3–5] by including the variations in interaction energy and hydrodynamic resistance coupled to the droplet deformation. The film between such small droplets will be much less prone to surface instabilities and corrugations like those discussed above. The reason is the greater capillary pressure inside the smaller droplets. Also, the smaller the formed film, the shorter the wavelengths of the allowed surface waves [52]. This leads to a greater energy penalty for local deformations. The latter also may include the "black spot" formation and subsequent film thinning mechanism suggested by Derjaguin *et al.* [45,53]. Thus, the film evolution and

*Also at Instituto Venezolano de Investigaciones Científicas (IVIC), Centro de Estudios Interdisciplinarios de la Física, Caracas, Venezuela.
†Corresponding author; dimiter@unm.edu

breakup pathways that are valid for large films are not likely to work for Brownian droplets that form small films.

The first attempt for theoretical analysis of Brownian droplet coalescence was performed by Danov *et al.* [22]. They considered the case of steady-state approach of two droplets that can deform and form a thin film at small separations. The shapes of the deformed droplets were approximated with those of truncated spheres that were separated by a plane-parallel liquid film. This approximation was analyzed in detail by comparing its results for the interaction energies with those obtained using the actual interfacial droplet shape [54]. It was demonstrated that the error in the energies introduced by the model shape is less than a few percent. The truncated sphere model was later used to obtain various thermodynamic properties of emulsions [30,31,55,56]. Another assumption adopted in Ref. [22] implies that the film between the droplets forms at a certain distance and does not change its radius during the subsequent stages of thinning and coalescence. This hypothesis was not supported by rigorous arguments but was employed as a simplification of an already difficult mathematical problem [22]. In fact, it is very likely that small films between Brownian droplets will be subjected to thermal disturbances due to the finite temperature of the system. As a result, both the film radius and thickness will fluctuate. The concept of a fluctuating cylindrical surface has been previously used in the study of carbon nanotubes [57].

In this paper, we offer a more general approach that does not limit the film radius to a constant value during the droplet approach and coalescence. Instead, the film radius and thickness variations are traced by employing Brownian dynamics analysis using the Langevin equations [58]. This method provides detailed insight into the film time evolution. There is no current experimental technique that allows to directly observing the film formation and time change for small (micrometer and submicrometer) Brownian droplets. Consequently, the proposed analysis presents a convenient and unique tool for examining the dependence of the droplet coalescence kinetics on parameters such as size, interfacial tension and mobility, charge, electrolyte concentration, etc. The obtained results have not only fundamental significance but are also relevant to industrial applications that involve formulation and processing of emulsions.

The stochastic nature of the film formation between two Brownian droplets requires a probabilistic description. The focus of the paper is on oil droplets in water, but the approach can be easily modified to include water droplets in oil. The next section briefly outlines the Fokker-Planck-Smoluchowski formalism that defines a time-dependent configurational probability for two approaching Brownian droplets. The cases of large and small interdroplet separations and the transition between them are discussed. A set of Langevin equations that correspond to the Smoluchowski probability differential equation are derived. They are used to trace the film radius and thickness time evolution. The numerical procedure for the Brownian dynamics simulation is described in Sec. III. In Sec. IV, we discuss results and Sec. V concludes with a summary.

II. THEORETICAL BACKGROUND

A. Smoluchowski analysis of two approaching droplets

The Smoluchowski equation is a special case of the more general Fokker-Planck equation [59]. It applies to the situation when the Brownian particle experiences high viscous friction with the solvent [60]. It also applies to systems that have almost reached thermal equilibrium, but not the configurational equilibrium and there are fluxes due to the gradient diffusion. Hence, if the Brownian dispersion is almost in thermal equilibrium Fokker-Planck equation for N particles suspended in a viscous solvent can be reduced to the Smoluchowski equation [61]. For two Brownian droplets in viscous solvent moving relative to each other, the Smoluchowski equation is

$$\frac{\partial P(\mathbf{r})}{\partial t} = \nabla \cdot \mathbf{D}(\mathbf{r}) \cdot \left(\nabla P(\mathbf{r}) + \frac{1}{k_B T} P \nabla W(\mathbf{r}) \right), \tag{1}$$

where $P(\mathbf{r})$ is the configuration probability function in Cartesian space and time t, and $k_B T$ is the thermal energy. The direct thermodynamic interactions between the two droplets are included in the force term $F(\mathbf{r}) = -\nabla W(\mathbf{r})$, while the hydrodynamic forces are taken into account by the diffusion tensor $\mathbf{D}(\mathbf{r})$.

At large separations the droplets are spherical; and, if their interfacial mobility is negligible, the diffusion tensor can be expressed in the form [63]

$$D_{ii} = D_0 \delta_{ii} + D_0 \sum_{j=1, j \neq i} [A_s \hat{r}_{ij} \hat{r}_{ij} + B_s (\delta_{ii} - \hat{r}_{ij} \hat{r}_{ij})], \tag{2}$$

$$D_{ij} = D_0 [A_c \hat{r}_{ij} \hat{r}_{ij} + B_c (\delta_{ii} - \hat{r}_{ij} \hat{r}_{ij})], \tag{3}$$

where $\hat{r}_{ij} = (r_j - r_i)/|r_{ij}|$ is the radius vector between the centers of the two spheres and δ_{ii} are the components of the unit tensor. D_{ii} refers to the self-diffusion, while D_{ij} accounts for the effect of the hydrodynamic interactions between particles i and j. The functions A_s, B_s, A_c, and B_c depend on the distance between the particles [62]. Different forms of these functions were suggested by Felderhof, Oseen, Rotne-Prager, and Batchelor [62–64]. This method was utilized in Ref. [65] to calculate the time for droplet approach. However, the analysis showed that it fails at short separations and/or when many particles are involved in the collision. In the former case, one needs to account for the droplet deformation and to consider the hydrodynamics in the lubrication limit. Such an analysis was performed in Ref. [23]. In this case, the Smoluchowski equation describes the probability for the existence of a disk-shaped thin liquid film with radius r and thickness h at moment t between the two droplets [see Fig. 1(a)],

$$\frac{\partial P(r,h,t)}{\partial t} = \nabla \cdot \left\{ \mathbf{D}(r,h) \cdot \left[\nabla P(r,h,t) + \frac{P(r,h,t)}{k_B T} \nabla W(r,h) \right] \right\}. \tag{4}$$

Note that Eqs. (1) and (4) refer to two different processes. The former describes the relative motion of two spherical particles (or droplets) in three-dimensional Cartesian space. The droplet deformation is not taken into account and the

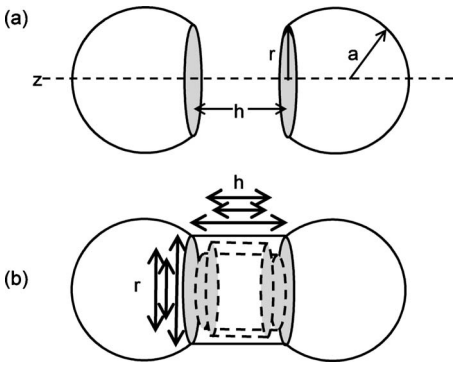

FIG. 1. (a) Truncated sphere model adopted to emulate the deformation process during the collision of two emulsion droplets. Note the cylindrical geometry exhibited by the film of radius r and thickness h. (b) Schematic representation of the random configurations which may adopt the film parameters r and h during a particular stage in the process of thinning. Film parameters shown were exaggerated for a better visualization.

phase space does not include the film radius. Equation (4) was derived to analyze the approach of two droplets along the line connecting their centers (i.e., the z coordinate). Hence, it does not take into account the full relative droplet motion in three-dimensional space, but instead traces the evolution of the thin liquid film when both its thickness h and radius r can exhibit random variations in the r-h plane [see Fig. 1(b)]. The phase space for Eq. (4) is two dimensional and consists of the film radius and thickness.

All the direct thermodynamic interactions are incorporated in the potential W. These may include van der Waals, electrostatic, steric, and hydrophobic forces. The direct interactions are shape dependent and, for deformed droplets approximated by truncated spheres, they are functions of the film radius r and thickness h [32,56,66]. The two-dimensional diffusion tensor in Eq. (4), in the lubrication limit, depends on r and h and is given by

$$\mathbf{D}(r,h) = k_B T \boldsymbol{\zeta}(r,h)^{-1}, \tag{5}$$

where the components of the friction tensor $\boldsymbol{\zeta}$ are [23]

$$\zeta_{rr}(r,h) = \frac{6\pi\eta r^2}{h(1-\epsilon_s)}, \tag{6}$$

$$\zeta_{hh}(r,h) = \frac{3\pi\eta a^2}{2h}\left(1 + \frac{r^2}{ah} + \frac{r^4}{a^2h^2}\right), \tag{7}$$

$$\zeta_{hr}(r,h) = \zeta_{rh} = -\frac{3\pi\eta r^3}{h^2}. \tag{8}$$

These components also depend on the droplet radius a and the solvent bulk dynamic viscosity η. ζ_{rr} is also a function of the parameter ϵ_s, which accounts for the tangential mobility of the droplet surfaces [22]. The values of this parameter may vary between ~0.001 and 1, depending on the surfactant [44]. Low values for ϵ_s mean high mobility, while $\epsilon_s = 1$ corresponds to tangentially immobile droplet surfaces. We should stress that $\nabla \cdot D \neq 0$ [see Eqs. (1) and (4)] and therefore the probability function will experience an additional force that is due to the variation of the hydrodynamic forces within the film [62,64].

If the film formed between the droplets thins down to a critical value h_{cr}, it will break and the droplets will coalesce [56]. Then the coalescence problem is reduced to finding the mean escape time τ from a domain with an absorbing boundary at $h=h_{cr}$ [60,67]. Equation (4) can be transformed into an equation for the escape time τ [23],

$$\nabla \cdot [P_{eq}(r,h)\mathbf{D}(r,h) \cdot \nabla \tau(r,h)] = -1, \tag{9}$$

where $P_{eq} = \exp[-W(r,h)/k_B T]$ is the equilibrium configuration probability function. Equation (9) can be used to find the time necessary to reach $h=h_{cr}$. It accounts for the fact that the film radius can fluctuate along with the film thickness and potentially contribute to the escape time τ. Below, we derive the set of Langevin stochastic differential equations which are amenable to computer simulation and offer a different route to obtain detailed information about the dynamics of droplet collisions, film formation, thinning, and coalescence.

B. Langevin dynamics of droplet collision

Langevin dynamics presents an alternative treatment of Brownian systems. Usually, there is a set of Langevin equations that correspond to any master differential equation for the time-dependent probability [60,67,68]. According to our analysis in the previous section, two approaching deformable droplets probe a two-dimensional configuration space defined by the film radius r and thickness h. The probability function for r and h is a solution of the Smoluchowski equation [Eq. (4)], which is a very good approximation for Brownian movements in the high friction limit. Our approach is based on the method developed by Ermak and McCammon [58] and is modified explicitly to account for the droplet surface fluidity and deformability. The representative coordinates for our system are the radius and thickness of the film formed as the droplets approach each other. The Langevin equations corresponding to Eq. (4), in the absence of inertial effects, read [see Fig. 1(b)]

$$\frac{dr}{dt} = \left(\frac{1}{r}\frac{\partial}{\partial r} r D_{rr} + \frac{\partial}{\partial h} D_{rh}\right) - \frac{1}{k_B T}\left(D_{rr}\frac{\partial W}{\partial r} + D_{rh}\frac{\partial W}{\partial h}\right) + \hat{v}_r(t), \tag{10}$$

$$\frac{dh}{dt} = \left(\frac{1}{r}\frac{\partial}{\partial r} r D_{rh} + \frac{\partial}{\partial h} D_{hh}\right) - \frac{1}{k_B T}\left(D_{hh}\frac{\partial W}{\partial h} + D_{rh}\frac{\partial W}{\partial r}\right) + \hat{v}_h(t). \tag{11}$$

The first two terms on the right-hand side of Eqs. (10) and (11) originate from the fact that $\nabla \cdot \mathbf{D} \neq 0$. They represent the directional drift velocities. The h component of directional forces opposes the droplet approach due to the increasing hydrodynamic resistance with the decreasing film thickness. The second terms on the right-hand sides of Eqs. (10) and (11) account for the thermodynamic direct interactions between the droplets (van der Waals, electrostatic, etc.) and can be positive or negative, depending on the position on the

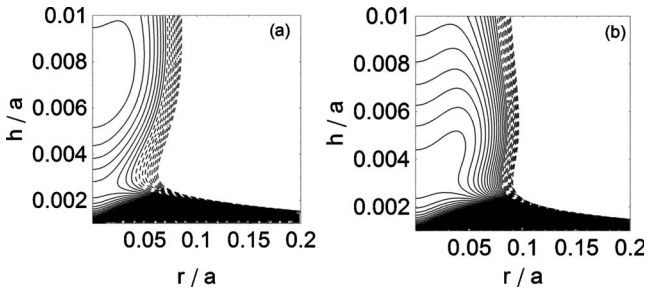

FIG. 2. Contour curves of interaction potential of two equal droplets (a=500 nm). The electrostatic surface potential is 15 mV and the interfacial tension is 4 mN/m. The separation between the lines is k_BT. The full lines correspond to negatives values of the energy while the dashed lines shown are for positive energies. (a) C_{el}=0.1 M and (b) C_{el}=0.2 M. As the droplets approach the energy surface may exhibit a far minimum which is better visible in (a). Further approach requires overcoming a saddle barrier before falling into the deep energy minimum at very short distances.

energy surface in the r-h space (see Fig. 2). The third terms, $\hat{v}_r(t)$ and $\hat{v}_h(t)$, represent the random velocities due to thermal fluctuations. The solvent is considered as a viscous continuum. Its effect on the process is included in the diffusion tensor components (through the viscosity) and the thermodynamic forces (through the dielectric permittivity and background electrolyte concentration—see below.)

The film configuration space is limited by the following boundary conditions. As the film thickness decreases, it may eventually reach the critical value h_{cr} where it breaks leading to droplet coalescence. Consequently, $h=h_{cr}$ defines an absorbing boundary. It can be estimated by means of the Vrij formula [69]

$$h_{cr} = 0.243\left(\frac{A_H^2 a^2 h_0}{2\pi\gamma^2}\right)^{1/7}, \tag{12}$$

where A_H is the Hamaker constant, h_0 is the distance at which the droplets start to deform, γ is the interfacial tension, and a is the droplet radius. According to Eq. (12) all films with thicknesses less than or equal to h_{cr} will be unstable and collapse due to an overwhelmingly strong van der Waals attraction (see also Ref. [22]).

The film radius cannot physically reach negative values. Therefore, r=0 is a reflecting boundary. On the other hand, values of the radii that are too large lead to an increasingly unfavorable extension energy and, hence, $P_{eq}(r\to\infty)\to 0$. If the droplet attraction is insufficient, they may move apart at the boundary $h\to\infty$. Our primary interest is to calculate the time necessary to reach the boundary $h=h_{cr}$ defined by Eq. (12).

C. Direct interactions between the droplets

The direct surface interactions between particles and droplets are due to electrostatic, van der Waals, depletion, hydration, or hydrophobic forces [70]. They are shape dependent and were analyzed in detail for the particular case of two deformable emulsion droplets. The model shape of two truncated spheres (see Fig. 1) allowed for the derivation of analytical expressions for the different possible contributions [56,66,71]. The film formation also leads to the appearance of interfacial tension (extension) and, in some cases, bending (local curvature change) energy contributions [66]. The overall interaction energy is a function of both the surface separation distance and the radius of the film formed between the droplets. Therefore, it is represented by a two-dimensional surface (see Fig. 2).

The droplets may (or may not) be stabilized with adding surfactant. In both cases the van der Waals attraction is [56]

$$W_{vdW}(r,h) = -\frac{A_H}{12}\left(\frac{4a^2}{(2a+h)^2} + \frac{4a^2}{h(4a+h)} + 2\ln\left[\frac{h(4a+h)}{(2a+h)^2}\right] + \frac{128a^5r^2}{h^2(2a+h)^3(4a+h)^2}\right). \tag{13}$$

Electrostatic repulsion is usually due to the presence of an ionic surfactant that adsorbs at the droplet interface. At moderately high (<25 mV) and constant surface potential Ψ_0, the electrostatic energy between two truncated spheres is given by [56]

$$W_{el}(r,h) = \pi\epsilon_0\epsilon\kappa\Psi_0^2\{[1-\tanh(\kappa h/2)]r^2 + 2a\kappa^{-1}\ln[1+\exp(-\kappa h)]\}, \tag{14}$$

where $\kappa^{-1}=(2e^2z^2C_{el}/\epsilon_0\epsilon k_BT)$ is the screening Debye length for symmetric (z:z) electrolyte (z being the ionic charge number), e=1.602 10×10^{-19} C is the electron charge, ϵ_0 =8.85$\times10^{-12}$ F m^{-1} is the vacuum permittivity, and ϵ =80.4 is the relative dielectric constant of water at room temperature. Higher surface potential (or charge) leads to more stable droplets. This is due to the increased electrostatic repulsion. The effect of the surface potential and/or charge on the interaction energy between deformable droplets has been extensively studied in the past [22,32,54–56,66].

The energy due to the surface extension is given by [56]

$$W_{ext}(r) = \frac{1}{2}\pi\gamma\frac{r^4}{a^2}, \tag{15}$$

where γ is the interfacial tension. Thus, the total energy of interaction is $W(r,h)=W_{vdW}+W_{el}+W_{ext}$. Other energy contributions such as depletion, structural, and steric could be easily incorporated if present [66]. The expressions for the electrostatic and extension energies as well as the friction tensor were derived assuming moderate droplet deformation (r/a $\leq$0.3) [22].

III. NUMERICAL PROCEDURE

The Langevin equations (10) and (11) have to be written in a finite difference form,

$$\Delta r = \left(\frac{1}{r}\frac{\partial}{\partial r}rD_{rr} + \frac{\partial}{\partial h}D_{rh}\right)^0\Delta t - \frac{1}{k_BT}\left(D_{rr}\frac{\partial W}{\partial r} + D_{rh}\frac{\partial W}{\partial h}\right)^0\Delta t + \Re(\Delta t), \tag{16}$$

$$\Delta h = \left(\frac{1}{r}\frac{\partial}{\partial r} r D_{rh} + \frac{\partial}{\partial h} D_{hh}\right)^0 \Delta t - \frac{1}{k_B T}\left(D_{hh}\frac{\partial W}{\partial h} + D_{rh}\frac{\partial W}{\partial r}\right)^0 \Delta t + \mathfrak{H}(\Delta t). \tag{17}$$

Equations (16) and (17) describe the dynamics of a thin liquid film formed between two droplets in the configurational space of the radii and thicknesses. They can be solved following the procedure proposed by Ermak and McCammon [58]. The time step $\Delta t \gg m D_{ii}^0 / k_B T$ is selected in accordance with the Brownian dynamics analysis procedure for friction dominated systems. The superscript 0 refers to the value at the previous step. Ermak and McCammon [58] considered the relative motion of two spherical particles at large separations. Hence, they used the Oseen and Rotne-Prager diffusion tensors to account for the hydrodynamic interactions at large separations. Both Oseen and Rotne-Prager tensor have zero divergence, $\nabla \cdot \mathbf{D} = 0$, and the diffusion drift terms disappear from their equations. In contrast, we have to keep the first terms on the right-hand sides of Eqs. (16) and (17) because the diffusion tensor defined by Eqs. (5)–(8) has a nonzero divergence, $\nabla \cdot \mathbf{D} \neq 0$.

The displacements $\mathfrak{R}(\Delta t)$ and $\mathfrak{H}(\Delta t)$ are random variables that have to be obtained using a multivariate Gaussian distribution [58]. Because of the symmetry of the film between the droplets, the three-dimensional Gaussian distribution transforms into a combination of a Rayleigh and one-dimensional Gaussian distribution [72] (see also Appendixes A–C). Following the procedure described in Appendixes A–C, we generate random deviates that conform to the two distributions. They are then used to obtain the actual physical displacements in radial and normal direction using the expressions (see Refs. [58,73] for details)

$$\mathfrak{L}_i(\Delta t) = \sum_{j=1}^{i} \sigma_{ij} X_j \Delta t^{1/2}. \tag{18}$$

Here, $\mathfrak{L}_1 = \mathfrak{R}$ and $\mathfrak{L}_2 = \mathfrak{H}$, $X_1 = X_r$ and $X_2 = X_h$ are dimensionless Rayleigh or Gaussian random deviates [see Eq. (C3) in Appendix C], and σ_{ij} represents the weighting factors calculated from

$$\sigma_{ii} = \sqrt{D_{ii} - \sum_{k=1}^{i-1} \sigma_{ik}^2}, \tag{19}$$

$$\sigma_{ij} = \left(D_{ij} - \sum_{k=1}^{j-1} \sigma_{ik}\sigma_{jk}\right)\sigma_{jj}^{-1}, \quad i > j. \tag{20}$$

Equations (19) and (20) follow from the relationship between the covariance matrix and the diffusion tensor matrix [see Eq. (A3) in Appendix A]. This procedure accounts for the hydrodynamic coupling between the random fluctuations in the film thickness and radius [58,73].

IV. RESULTS AND DISCUSSION

This section presents results obtained by using the above procedure. The parameters used for the computations are $\Psi_0 = 15$ mV, $\epsilon = 80.4$, $\epsilon_0 = 8.85 \times 10^{12}$ Fm^{-1}, $\gamma = 4$ mN/m, $\eta = 8.91 \times 10^{-4}$ kg m^{-1} s^{-1}, $T = 298$ K, and $A_H = 4 \times 10^{-21}$ J. The mean coalescence times are obtained by averaging over a hundred independent numerical experiments with different initial values of seeds used to calculate the random displacements. The above parameters give a critical film thickness h_{cr} between 1 and 2 nm depending on the droplet radius [see Eq. (12)]. We use a value of 1 nm for all cases. The time step used for all calculations was $\Delta t = 1 \times 10^{-8}$ s. The initial droplet separation was selected to fulfill the lubrication approximation ($h_0 = 10$ nm). The selected initial film radius is 1 nm. Hence, we consider the final stages of film thinning and coalescence in the presence of complex surface interactions which depend on the electrolyte concentration. In addition to that, we examine the effect of tangential mobility on the coalescence time for two colliding Brownian droplets. This approach is complementary to the analysis previously done for large separations between the droplets [65]. Below we focus on the effects of interfacial mobility and droplet size on the film evolution and coalescence.

Figure 3 shows the configurations of the thin liquid film formed between two droplets in the r-h space. Figure 3(a) corresponds to $C_{el} = 0.1$ M and $\epsilon_s = 0.01$ [see also Fig. 2(a)]. The system remains trapped in the vicinity of the energy minimum around $h/a = 0.008$ and is kinetically stabilized against coalescence. Given enough time, the system would eventually cross the saddle point shown in Fig. 2(a) and will coalesce. However, for 5×10^6 iterations (i.e., ~50 ms) no coalescence was observed. Figure 3(b) corresponds to the same parameters of Fig. 3(a) but lower interfacial mobility ($\epsilon_s = 0.9$). For droplets with radius $a = 500$ nm and lower electrolyte concentration, the electrostatic repulsive barrier provides kinetic stability for the system. Increasing C_{el} decreases the electrostatic repulsion through screening and the preferred configurations correspond to lower film thicknesses. In the absence of an energy barrier [see Fig. 2(a)] to prevent coalescence, the main force resisting film thinning is due to viscous hydrodynamic resistance. The average coalescence time for this case [Fig. 3(c)] is $\tau \simeq 15$ ms. Lowering the surface mobility [see Fig. 3(d)] further increases the coalescence time by allowing the system to probe more configurations at larger separations. In this case, about 40% of the runs end with droplet coalescence with typical time $\tau \simeq 30$ ms. The remaining 60% do not reach coalescence within 50 ms. The surface mobility is more important for high electrolyte concentrations where the electrostatic interactions are screened and the droplets can get closer. Smaller separation between the droplets leads to greater shear stresses and, hence, greater viscous resistance to further approach. Increasing the surface mobility and allowing the interfaces to flow decrease these stresses. As a result, the viscous force also decreases and the droplets may approach even further. The hydrodynamic resistance plays an important role in the possible configurations of the film because it might "force" the system to spend more time in regions where the direct interaction energy is not necessarily minimal. The hydrodynamic effect is included in the term $\nabla \cdot \mathbf{D}$. Note that it depends not on the local values of the diffusion (or friction) tensor components, but on their spatial derivatives. Increasing the surface mobility lowers the viscous resistance, but at the same time increases the variations in the

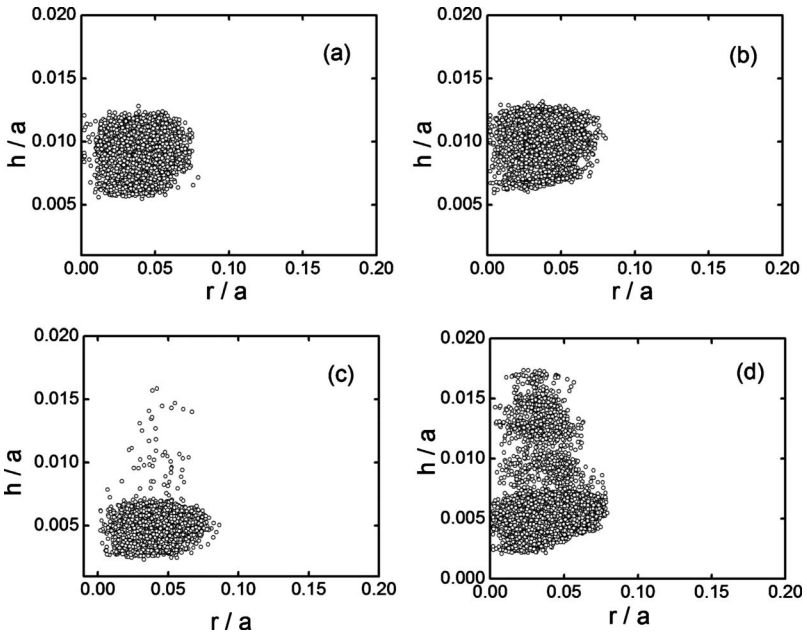

FIG. 3. Film configuration in r-h space. The particle radius is 500 nm, interfacial tension is 4 mN/m, and surface electrostatic potential is 15 mV. (a) C_{el}=0.1 M and ϵ_s=0.01; (b) C_{el} =0.1 M and ϵ_s=0.9; (c) C_{el}=0.2 M and ϵ_s =0.01; (d) C_{el}=0.2 M and ϵ_s=0.9.

stress with position, which may lead to greater values of $\nabla \cdot \mathbf{D}$.

Figure 4 provides further insight in the combined effect of direct surface and hydrodynamic interactions on the coalescence time discussed above. It depicts the h and r components of the deterministic velocity $(\nabla \cdot \mathbf{D} - \mathbf{D} \cdot \nabla W / k_B T)$ [see also Eqs. (10) and (11)]. Figures 4(a) and 4(b) correspond to electrolyte concentration of 0.1 M. The positive regions of the surfaces (above the horizontal planes) correspond to a deterministic increase in film thickness and/or radius. Coalescence would be possible only if the random term v_h in Eq. (11) is negative and large enough to overcome the positive velocity shown in Fig. 4(a). If the film radius $r/a > 0.08$, the directional forces in the h direction will favor the coalescence. However, the forces in r direction try to reduce the film radius in this region [see Fig. 4(b)]. Therefore, this route also requires a large velocity fluctuation, this time in the r direction. This leads to a lower overall coalescence probability for salt concentration equal to 0.1 M monovalent electrolyte.

Increasing the electrolyte concentration to 0.2 M does not substantially change the deterministic velocity in the r direction [see Fig. 4(d)]. However, it has a strong effect in the film thinning velocity [see Fig. 4(c)]. The velocity of spontaneous film growth due to the deterministic term in Eq. (11) is much slower and can be easily overcome by a velocity fluctuation (v_h) in the opposite direction. Hence, the film evolution and coalescence is governed by the combined effects of the complex interaction energy and hydrodynamic resistance.

The interplay between the direct interactions and surface mobility is also evident for smaller droplets. Figure 5 shows the coalescence times vs electrolyte concentration for four different interfacial mobilities and droplet radius a =100 nm. The curves show that the coalescence times significantly increase as the salt concentration and interfacial mobilities decrease. Low salt concentration leads to greater electrostatic repulsion, while low mobility of the droplet interfaces enhances the hydrodynamic drag upon approach. Smaller droplets are "harder" due to the higher internal capillary pressure. That is why they are less prone to deformation and film formation. The interaction energy surface for small droplets does not exhibit a minimum above a saddle barrier, like the one shown in Fig. 2(a). Therefore, the system is less likely to be trapped in metastable states similar to those in Figs. 3(a) and 3(b). The comparison of the different cases in Figs. 5(a)–5(d) shows that the effect of the salt is greater for droplets with less surface mobility. High surface mobilities reduce the hydrodynamic resistance, and the coalescence time depends mostly on the direct interactions. The repulsive part of these interactions is mainly due to the electrostatic energy. The addition of electrolyte screens the repulsion and decreases the coalescence time. Lower surface mobility leads to greater change in the coalescence times with the background salt concentration. Hence, for smaller and less deformable droplets, the lower the surface mobility the sharper the drop in the coalescence times with the increasing amount of electrolyte. This can be attributed to the fact that for too small separations (due to screened electrostatic repulsion) the van der Waals attraction becomes strong enough to overcome the friction resistance and reduces the film thickness to its critical value given by Eq. (12). The friction resistance is greater for deformable droplets. Therefore, smaller and harder droplets will experience weaker hydrodynamic interactions compared to larger and softer ones.

Replacing the ionic surfactants with nonionic ones may lead to droplets with no surface charge. In this case, there would be no electrostatic repulsion and energy barrier. The attraction will monotonously increase as the distance h becomes smaller. If the surfactants are soluble in the droplet phase, they can further reduce the hydrodynamic resistance by lowering the value of ϵ_s and destabilize the emulsion [44]. Figure 6 presents data for the film radius and thickness evolution with time for different combinations of interfacial tensions and mobilities. In principle, these can be controlled by selecting appropriate surfactants and their concentrations.

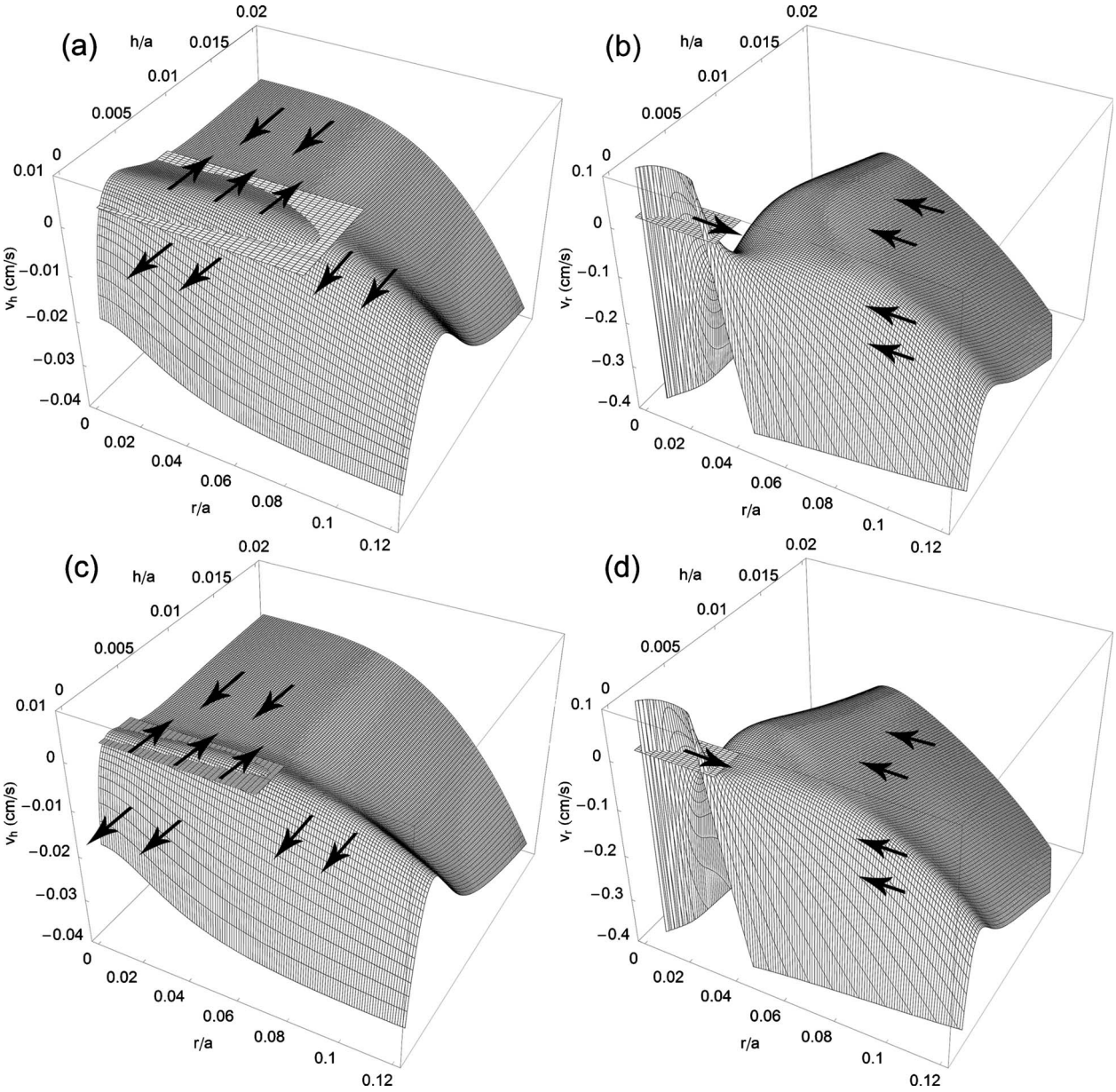

FIG. 4. Velocity vector ($\nabla\cdot\mathbf{D}-\mathbf{D}\cdot\nabla W/k_BT$). v_h is the h component [cases (a) and (c)] and v_r is the r component [cases (b) and (d)] The arrows show the direction of the velocity components. Top plots correspond to a electrolyte concentration of 0.1 M. Bottom plots correspond to the case of C_{el}=0.2 M. The values above the planes are positive (the film thickness and radius tend to grow). The values below the planes are negative (the film thickness and radius tend to decrease).

The plots represent typical examples of single Brownian dynamics runs. However, the coalescence times, shown in the figures, are very close to the average values that have been obtained from a hundred independent runs. Lower surface tension leads to greater average film radius, while higher interfacial mobility leads to greater amplitudes of the film fluctuations. Changing the interfacial mobilities from extremely mobile to almost immobile leads to an approximately twofold increase in the coalescence time. Interestingly, the film radius for the case of γ=1 mN/m and ϵ_s =0.9 reaches a plateau value, which is reproducible for almost all the cases that were studied. The lower amplitudes observed in the case of ϵ_S=0.9 are due to the fact that the surface is less susceptible to fluctuations because of the low surface mobility. On the contrary, the more mobile the surface is, the more sensitive it is to large amplitude fluctuations. According to these results, the film growth is not monotonous. The film radius exhibits random fluctuations around a mean value. As the interfacial tension increases, the mean value of the film radius decreases. This is expected since the interfacial tension opposes surface flattening of the droplets.

These are important results because they show that film formation between small Brownian droplets is different in comparison with larger millimeter drops. In the latter case, it was shown that the film evolves from zero radius up to $r_{max}=\sqrt{ah_0}$, where h_0 is the distance where the deformation starts [44]. While such a behavior was also assumed to be

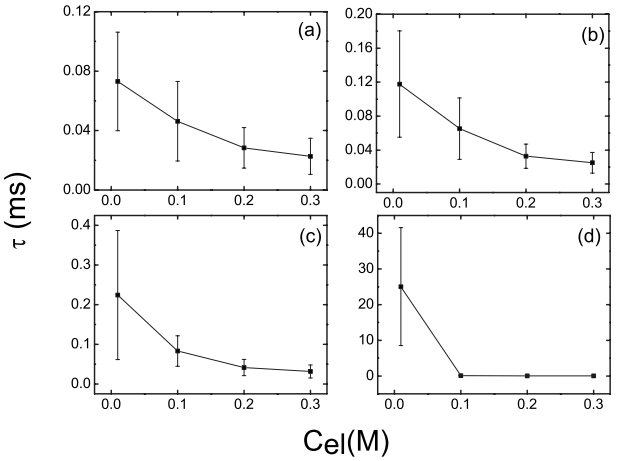

FIG. 5. Coalescence time τ vs electrolyte concentration C_{el} for different surface mobilities (a=100 nm): (a) ϵ_s=0.01, (b) ϵ_s=0.1, (c) ϵ_s=0.2, and (d) ϵ_s=0.4. The bars represent the standard deviation for 100 numerical experiments. The error bars for the last two data points in (d) are smaller than the point size.

valid for smaller droplets [22], our results show that this is not correct.

The average coalescence time vs droplet radius is shown in Fig. 7. The interfacial mobility is high (ϵ_S=0.01), and the droplets are uncharged. Hence, the coalescence kinetics depends on the van der Waals attraction and the hydrodynamic resistance. Both interactions increase with the droplet size, but the effect is stronger for the hydrodynamics. Larger droplets are more deformable and form larger plane parallel films at approach. The hydrodynamic resistance for squeezing the fluid out of larger films is greater and, hence, the coalescence time is longer. As a result, the coalescence times show a nonlinear increase with the droplet size. In contrast, the original Smoluchowski theory [3–5] does not account for any size dependence of the coagulation kinetics because any long-range thermodynamic and hydrodynamic interactions are not taken into account.

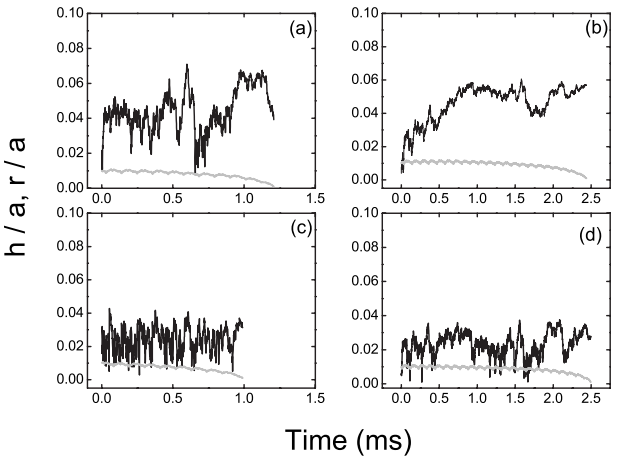

FIG. 6. Time evolution of the film thickness h (gray lines) and film radius r (black lines) formed between two deformable droplets (a=1 μm) in the absence of electrical surface charge. (a) γ =1 mN/M and ϵ_s=0.01, (b) γ=1 mN/M and ϵ_s=0.9, (c) γ =10 mN/M and ϵ_s=0.01, and (d) γ=10 mN/M and ϵ_s=0.9.

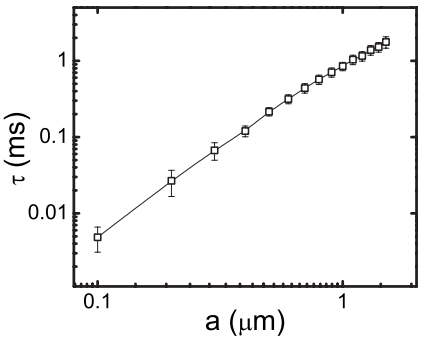

FIG. 7. Dependence of the coalescence time on the droplet radius in the absence of surface charge (ϵ_s=0.01); γ=50 mN/m. The error bars represent standard deviation on 100 numerical experiments.

V. CONCLUDING REMARKS

Emulsion film formation and its time evolution is a complex event. It is strongly affected by the thermodynamic and hydrodynamic interactions between the droplets in combination with the random Brownian disturbances from the surrounding medium. Small droplets and liquid films can be described using Langevin dynamics. This approach allows us to account for all the forces acting on the colliding droplets and to obtain the film formation evolution and coalescence time. We have shown that the effect of the tangential mobility on the coalescence time is extremely important and is coupled to the effect of the direct thermodynamic interactions. The hydrodynamic interactions lead to an effective force that pulls the droplets apart. This effect is stronger for droplets with less tangentially mobile interfaces. High tangential mobility facilitates the coalescence while low values of mobilities oppose droplet fusion by increasing the viscous resistance and slowing the film thinning time. Droplets with lower surface mobilities are more sensitive to increasing the background electrolyte concentration, which reduces the coalescence time. The amplitude of the radial fluctuations is a strong function of the surface mobility. Lower mobilities lead to smaller amplitudes, and vice versa. Our analysis is valid for small droplet separations (in lubrication approximation) and moderate deformations. Therefore, it is complementary to other models that consider droplet approach from large distances [65] but ignore details in the hydrodynamics and surface forces that dominate the process at close proximity.

ACKNOWLEDGMENTS

We thank Dr. Boian Alexandrov for his helpful advice during the initial stages of this work. We also thank Dr. Boris Kiefer for reading the manuscript and providing valuable comments and suggestions. This research was financially supported by NSF CARRER CBET Contract No. 0844645, DOE-EERE, and DOE-EPSCoR implementation program: Materials for energy conversion.

APPENDIX A: CONFIGURATIONAL PROBABILITY IN 3D CARTESIAN COORDINATES: A BRIEF OVERVIEW

The probability density for the distribution of random deviates associated with Brownian motion in three-dimensional

Cartesian space is given by the normal Gaussian distribution [67,74],

$$f(\mathbf{r};t) = \frac{1}{(2\pi t)^{3/2}(\det|\mathbf{D}|t)^{1/2}} \exp\left(-\frac{\mathbf{r}^t \cdot \mathbf{D}^{-1} \cdot \mathbf{r}}{4t}\right), \quad \text{(A1)}$$

where $\mathbf{r}$ is the position vector, t is time, and $\mathbf{D}=k_BT\boldsymbol{\zeta}^{-1}$ is the diffusion tensor [see Eq. (5) in the text]. The denominator is derived from the normalization condition

$$\int_{-\infty}^{\infty} f(\mathbf{r};t)d\mathbf{r} = 1. \quad \text{(A2)}$$

If hydrodynamic interactions are present, the random terms in the Langevin equations for the different coordinates are correlated. To account for the hydrodynamic interactions, Ermak and McCammon [58] used a Cholesky decomposition [75] of the diffusion (or friction) tensor assuming the existence of lower triangular matrix $\boldsymbol{\sigma}$ and its conjugate transpose $\boldsymbol{\sigma}^T$, which are defined by the variance

$$\boldsymbol{\sigma}\boldsymbol{\sigma}^T = \mathbf{D}. \quad \text{(A3)}$$

The procedure for generating normal deviates that are distributed according to Eq. (A1), as well as their relationship to the actual physical displacements (through the matrix $\boldsymbol{\sigma}$), is explained in detail in Appendix G, part 3 in Ref. [73] (see also below).

APPENDIX B: DIFFUSION AND FRICTION TENSORS IN POLAR CYLINDRICAL COORDINATES

The starting point of our derivation of the diffusion and friction tensors in cylindrical coordinates is the product

$$\mathbf{r}^T \cdot \mathbf{D}^{-1} \cdot \mathbf{r} = \mathbf{D} = \frac{\mathbf{r}^T \cdot \boldsymbol{\zeta} \cdot \mathbf{r}}{k_BT}. \quad \text{(B1)}$$

The expanded form of Eq. (B1) in Cartesian coordinates reads

$$\mathbf{r}^T \cdot \boldsymbol{\zeta} \cdot \mathbf{r} = \zeta_{xx}x^2 + \zeta_{yy}y^2 + \zeta_{zz}z^2 + 2\zeta_{xy}xy + 2\zeta_{xz}xz + 2\zeta_{yz}yz. \quad \text{(B2)}$$

The next step is to transform the coordinates and the tensor matrix elements from Cartesian to cylindrical. The cylindrical coordinates are defined by [76] (see also Fig. 1)

$$x = r\cos\theta, \quad y = r\sin\theta, \quad z = h. \quad \text{(B3)}$$

For convenience, we will transform $\boldsymbol{\zeta}$ instead of $\mathbf{D}$ according to the expression [76]

$$\zeta_{ij}^{cart} = \sum_k \sum_l \frac{\partial q_k}{\partial q_i'} \frac{\partial q_l}{\partial q_j'} \zeta_{kl}^{cyl}, \quad \text{(B4)}$$

where q_k, q_l are the polar and q_i', q_j' are the Cartesian coordinates $(k,l=r,\theta,h;\ i,j=x,y,z)$. The superscripts "*cart*"and "*cyl*" refer to the Cartesian and cylindrical components of the friction tensor, respectively. Equation (B4) implies a covariant transformation. Contravariant or mixed transformations of the friction tensor from Cartesian to cylindrical will lead to the same results. Introducing the results from Eq. (B4) into Eq. (B2) and after tedious but straightforward calculations we obtain

$$\mathbf{r}^T \cdot \boldsymbol{\zeta}^{cart} \cdot \mathbf{r} = \zeta_{rr}^2 r^2 + \zeta_{hh}^2 h^2 + \zeta_{rh}^2 rh = \mathbf{r}^T \cdot \boldsymbol{\zeta}^{cyl} \cdot \mathbf{r}, \quad \text{(B5)}$$

where

$$\boldsymbol{\zeta}^{cart} = \begin{pmatrix} \zeta_{xx} & \zeta_{xy} & \zeta_{xz} \\ \zeta_{yx} & \zeta_{yy} & \zeta_{yz} \\ \zeta_{zx} & \zeta_{zy} & \zeta_{zz} \end{pmatrix}, \quad \text{(B6)}$$

$$\boldsymbol{\zeta}^{cyl} = \begin{pmatrix} \zeta_{rr} & \zeta_{rh} \\ \zeta_{hr} & \zeta_{hh} \end{pmatrix}. \quad \text{(B7)}$$

Note that the cylindrical symmetry of the problem lowers the matrix rank down to 2. The diffusion tensor in cylindrical coordinates is then

$$\mathbf{D}^{cyl} = k_BT(\zeta^{cyl})^{-1} = \begin{pmatrix} D_{rr} & D_{rh} \\ D_{hr} & D_{zz} \end{pmatrix}, \quad \text{(B8)}$$

which is the used one in Eqs. (16)–(20) . Both the friction and diffusion tensors are symmetric, i.e., $\zeta_{rh}=\zeta_{hr}$ and $D_{rh}=D_{hr}$.

APPENDIX C: PROBABILITY DISTRIBUTION AND RANDOM NUMBERS IN CYLINDRICAL SYMMETRY

The elementary volume in cylindrical coordinates is

$$d\mathbf{r} = 2\pi r dr dh, \quad \text{(C1)}$$

then [see Eq. (B5)]

$$f(\mathbf{r};t)d\mathbf{r} = \frac{r\exp\left(-\frac{\zeta_{rr}r^2 + \zeta_{hh}h^2 + \zeta_{rh}rh}{4k_BTt}\right)drdh}{\int_0^{\infty}\int_{-\infty}^{\infty}\exp\left(-\frac{\zeta_{rr}r^2 + \zeta_{hh}h^2 + \zeta_{rh}rh}{4k_BTt}\right)drdh}. \quad \text{(C2)}$$

This distribution is the basis that we use to generate our random displacements in the Langevin equations. It implies using a Rayleigh distribution for r and a Gaussian distribution for h (see Fig. 1). Following the procedure outlined in Refs. [58,73], we generate random deviates using distributions with unit variances

$$\tilde{f}(X_r) = X_r \exp\left(-\frac{X_r^2}{2}\right),$$

$$\tilde{f}(X_h) = \exp\left(-\frac{X_h^2}{2}\right). \quad \text{(C3)}$$

The Gaussian random deviates were generated using a standard Box-Müller algorithm [73,77,78]. The Rayleigh random deviates were also generated following the Box-Müller method [77] (see also Ref. [79]). The normal Gaussian deviates are obtained from

$$X_{h1} = \sqrt{-2\ln\xi_1}\cos(2\pi\xi_2),$$

$$X_{h2} = \sqrt{-2\ln\xi_1}\sin(2\pi\xi_2). \quad \text{(C4)}$$

The Rayleigh deviates are generated by using

$$X_r = \pm\sqrt{-2\ln\xi}. \tag{C5}$$

The variables ξ, ξ_1, and ξ_2 are uniformly distributed random numbers between 0 and 1. The right-hand side of Eq. (C5) can be positive or negative corresponding to positive or negative contribution fluctuation contribution to the film radius. We select the sign by generating a uniform random number in the range between 0 and 1. If the random number is less that 0.5 the positive sign is selected. If the random number is greater than 0.5 the then negative sign is chosen.

The generated random deviates X_r and X_h are not the actual displacements in the Langevin equations, although they are related to them. To obtain the physical displacements, we have to insert the obtained deviates in Eq. (18). The correlation between the r and h components, due to the hydrodynamic interactions, is taken into account by Eqs. (19) and (20) (see Refs. [58,73]).

[1] D. F. Evans and H. Wennestrom, *The Colloidal Domain: Where Physics, Chemistry, Biology, and Technology Meet* (Wiley, New York, 1999).
[2] P. Snabre and P. Mills, Eur. Phys. J. B **1**, 105 (2000).
[3] M. Smoluchowski, Phys. Z. **17**, 557 (1916).
[4] M. Smoluchowski, Phys. Z. **17**, 785 (1916).
[5] M. Smoluchowski, Z. Phys. Chem. **92**, 129 (1917).
[6] F. C. Collins and G. E. Kimball, J. Colloid Sci. **4**, 425 (1949).
[7] D. F. Calef and J. M. Deutch, Annu. Rev. Phys. Chem. **34**, 493 (1983).
[8] G. H. Weiss, J. Stat. Phys. **42**, 3 (1986).
[9] J. Keizer, Chem. Rev. **87**, 167 (1987).
[10] P. M. Debye, Trans. Electrochem. Soc. **82**, 265 (1942).
[11] N. A. Fuchs, Z. Phys. **89**, 736 (1934).
[12] J. M. Deutch and B. U. Felderhof, J. Chem. Phys. **59**, 1669 (1973).
[13] A. A. Ovchinnikov, S. F. Timasheff, and A. A. Belyy, *Kinetics of Diffusion Controlled Chemical Processes* (Nova Scientific, New York, 1989).
[14] B. V. Derjaguin, *Theory of Stability of Colloids and Thin Films* (Plenum Press, New York, 1989).
[15] T. R. Waite, Phys. Rev. **107**, 463 (1957).
[16] T. R. Waite, J. Chem. Phys. **28**, 103 (1958).
[17] G. Wilemski and M. Fixman, J. Chem. Phys. **58**, 4009 (1973).
[18] V. M. Titulaer, Physica A **100**, 251 (1980).
[19] D. G. A. L. Aarts and H. N. W. Lekkerkerker, J. Fluid Mech. **606**, 275 (2008).
[20] P. Meakin, Rep. Prog. Phys. **55**, 157 (1992).
[21] S. Kaur and L. G. Leal, Phys. Fluids **21**, 072101 (2009).
[22] K. D. Danov, N. D. Denkov, D. N. Petsev, I. B. Ivanov, and R. Borwankar, Langmuir **9**, 1731 (1993).
[23] D. N. Petsev, Langmuir **16**, 2093 (2000).
[24] X. Q. Xing, D. L. Butler, S. H. Ng, Z. Wang, S. Danyluk, and C. Yang, J. Colloid Interface Sci. **311**, 609 (2007).
[25] D. G. A. L. Aarts, H. N. W. Lekkerkerker, H. Guo, G. H. Wegdam, and D. Bonn, Phys. Rev. Lett. **95**, 164503 (2005).
[26] J. A. M. H. Hofman and H. N. Stein, J. Colloid Interface Sci. **147**, 508 (1991).
[27] I. U. Vakarelski, A. Toritani, M. Nakayama, and K. Higashitani, Langmuir **19**, 110 (2003).
[28] G. B. Webber, S. A. Edwards, G. W. Stevens, F. Grieser, R. R. Dagastine, and D. Y. C. Chan, Soft Mater. **4**, 1270 (2008).
[29] S. S. Dukhin, N. N. Rulev, and D. S. Dimitrov, *Coagulation and Dynamics of Thin Films* (Dumka, Kiev, 1980).
[30] D. N. Petsev, Physica A **250**, 115 (1998).
[31] D. N. Petsev and P. Linse, Phys. Rev. E **55**, 586 (1997).
[32] D. N. Petsev, in *Modern Aspects of Emulsion Science*, edited by B. P. Binks (Royal Society of Chemistry, London, 1998).
[33] G. Urbina-Villalba, J. Toro-Mendoza, A. Lozsan, and M. Garcia-Sucre, in *Emulsions: Structure, Stability and Interactions*, edited by D. N. Petsev (Elsevier, Amsterdam, 2004).
[34] J. Toro-Mendoza, A. Lozsan, M. Garcia-Sucre, A. J. Castellanos S., and G. Urbina-Villalba, Phys. Rev. E **81**, 011405 (2010).
[35] N. A. Mishchuk, S. V. Verbich, and S. S. Dukhin, J. Dispersion Sci. Technol. **18**, 517 (1997).
[36] S. S. Dukhin, J. Sjoblom, D. T. Wasan, and O. Saether, Colloids Surf., A **180**, 223 (2001).
[37] O. Holt, O. Saether, J. Sjoblom, S. S. Dukhin, and N. A. Mishchuk, Colloids Surf., A **123-124**, 195 (1997).
[38] S. Dukhin and J. Sjoblom, in *Emulsions and Emulsion Stability*, edited by J. Sjoblom (Marcel Dekker, New York, 1996).
[39] X. Zhang and R. H. Davis, J. Fluid Mech. **230**, 479 (1991).
[40] T. F. Tadros and B. Vincent, in *Encyclopedia of Emulsion Technology*, edited by P. Becher (Marcel Dekker, New York, 1983).
[41] D. Kashchiev and D. Exerowa, J. Colloid Interface Sci. **330**, 404 (2009).
[42] D. Kashchiev and D. Exerowa, J. Colloid Interface Sci. **203**, 146 (1998).
[43] R. Tsekov and E. Ruckenstein, Langmuir **9**, 3264 (1993).
[44] I. Ivanov and D. Dimitrov, in *Thin Liquids Films*, edited by I. B. Ivanov (Marcel Dekker, New York, 1988).
[45] B. V. Derjaguin and A. V. Prokhorov, J. Colloid Interface Sci. **81**, 108 (1981).
[46] M. G. Velarde and M. Vignes-Adler, in *Encyclopedia of Surface and Colloid Science*, edited by A. T. Hubbard (Marcel Dekker, New York, 2002).
[47] V. W. A. de Villeneuve, J. M. J. van Leeuwen, W. van Saarloos, and H. N. W. Lekkerkerker, J. Chem. Phys. **129**, 164710 (2008).
[48] V. W. A. de Villeneuve, J. M. J. van Leeuwen, J. W. J. de Folter, D. G. A. L. Aarts, W. van Saarloos, and H. N. W. Lekkerkerker, EPL **81**, 60004 (2008).
[49] S. T. Milner and S. A. Safran, Phys. Rev. A **36**, 4371 (1987).
[50] H. Gang, A. H. Krall, and D. A. Weitz, Phys. Rev. E **52**, 6289 (1995).
[51] H. Gang, A. H. Krall, and D. A. Weitz, Phys. Rev. Lett. **73**, 3435 (1994).
[52] E. Manev and A. Nguyen, Adv. Colloid Interface Sci. **114-115**, 133 (2005).
[53] B. V. Derjaguin and Y. V. Gutop, Kolloidn. Zh. **24**, 431

(1962).
[54] N. D. Denkov, D. N. Petsev, and K. D. Danov, J. Colloid Interface Sci. **176**, 189 (1995).
[55] N. D. Denkov, D. N. Petsev, and K. D. Danov, Phys. Rev. Lett. **71**, 3226 (1993).
[56] K. Danov, D. Petsev, N. Denkov, and R. Borwankar, J. Chem. Phys. **99**, 7179 (1993).
[57] C. H. Zhang, F. Kassubek, and C. A. Stafford, Phys. Rev. B **68**, 165414 (2003).
[58] D. L. Ermak and J. A. McCammon, J. Chem. Phys. **69**, 1352 (1978).
[59] R. J. A. Tough, P. N. Pusey, H. N. W. Lekkerkerker, and C. van den Broeck, Mol. Phys. **59**, 595 (1986).
[60] N. G. van Kampen, *Stochastic Processes in Physics and Chemistry* (Elsevier, New York, 1992).
[61] T. J. Murphy and J. L. Aguirre, J. Chem. Phys. **57**, 2098 (1972).
[62] W. B. Russel, D. A. Saville, and W. R. Schowalter, *Colloidal Dispersions* (Cambridge University Press, Cambridge, England, 1999).
[63] J. K. G. Dhont, *An Introduction of Dynamics of Colloids* (Elsevier, Amsterdam, 1996).
[64] B. U. Felderhof, Physica A **151**, 1 (1988).
[65] G. Urbina-Villalba, M. Garcia-Sucre, and J. Toro-Mendoza, Phys. Rev. E **68**, 061408 (2003).
[66] D. N. Petsev, N. D. Denkov, and P. A. Kralchevsky, J. Colloid Interface Sci. **176**, 201 (1995).
[67] C. W. Gardiner, *Handbook of Stochastic Methods: For Physics, Chemistry and Natural Science* (Springer, Berlin, 2004).
[68] R. Zwanzig, *Nonequilibrium Statistical Mechanics* (Oxford University Press, Oxford, 2001).
[69] A. Vrij, F. Hesselink, J. Luccasen, and M. van den Temple, Proc. K. Ned. Akad. Wet., Ser. B: Phys. Sci. **73**, 124 (1970).
[70] J. Israelachvili, *Intermolecular and Surface Forces* (Academic Press, London, 1992).
[71] J. K. Klahn, W. G. M. Agterof, F. V. Vader, R. D. Groot, and F. Groeneweg, Colloids Surf. **65**, 151 (1992).
[72] D. McQuarrie, *Mathematical Methods for Scientists and Engineers* (University Science Books, Sausalito, 2003).
[73] M. P. Allen and D. J. Tildesley, *Computer Simulations of Liquids* (Oxford University Press, New York, 1999).
[74] W. T. Coffey, Y. P. Kalmykov, and J. T. Waldron, *The Langevin Equation* (World Scientific, New Jersey, 2004).
[75] W. H. Press, S. A. Teukolsky, W. T. Vetterling, and B. P. Flannery, *Numerical Recipes in Fortran 77: The Art of Scientific Computing* (Cambridge University Press, New York, 1992).
[76] G. B. Arfken and H. J. Weber, *Mathematical Methods for Physicist* (Elsevier, Oxford, 2005).
[77] G. E. P. Box and M. E. Muller, Ann. Math. Stat. **29**, 610 (1958).
[78] Y. L. Tong, *The Multivariate Normal Distribution* (Springer-Verlag, New York, 1990).
[79] V. C. Lakhan, Math. Geol. **13**, 345 (1981).